Chem Biol Drug Des 2010; **76:** 245–254

Research Article

doi: 10.1111/j.1747-0285.2010.01006.x

Molecular Docking and QSAR Studies on Substituted Acyl(thio)urea and Thiadiazolo [2,3-α] Pyrimidine Derivatives as Potent Inhibitors of Influenza Virus Neuraminidase

Jiaying Sun[1,2,*], Shaoxi Cai[1,2], Hu Mei[1,2,*], Jian Li[2], Ning Yan[2], Qin Wang[2], Zhihua Lin[3] and Danqun Huo[1,2]

[1]*College of Bioengineering, Chongqing University, Chongqing 400044, China*

[2]*Key Laboratory of biorheological science and technology of Educational Ministry (Chongqing University), Chongqing 400044, China*

[3]*College of Chemistry and Bioengineering, Chongqing Institute of Technology, Chongqing 400050, China*

**Corresponding authors: Jiaying Sun, wy7472@126.com; Hu Mei, meihu@cqu.edu.cn*

Surflex–Dock was employed to dock 36 thiourea and thiadiazolo [2,3-α] pyrimidine derivatives into neuraminidase 1a4g. Molecular docking results showed that hydrogen bonding, electrostatic, and hydrophobic features were important factors affecting inhibitory activities of these neuraminidase inhibitors. Moreover, there was a significant correlation between the predicted binding affinity (total scores) and experimental pIC_{50} values with correlation coefficient $r = 0.846$ and $p < 0.0001$. Hologram quantitative structure–activity relationship, comparative molecular field analysis, and comparative molecular similarity indices analysis were used to develop quantitative structure–activity relationship models. Squared multiple correlation coefficients (r^2) of hologram quantitative structure–activity relationship, comparative molecular field analysis, and comparative molecular similarity indices analysis models were 0.899, 0.878, and 0.865, respectively. Squared cross-validated correlation coefficient (q^2) of hologram quantitative structure–activity relationship, comparative molecular field analysis, and comparative molecular similarity indices analysis models was in turn 0.628, 0.656, and 0.509. In addition, squared multiple correlation coefficients for test set (r^2_{test}) of hologram quantitative structure–activity relationship, comparative molecular field analysis, and comparative molecular similarity indices analysis models were 0.558, 0.667, and 0.566, respectively. The most active sample ID 2 was taken as a template molecule to design new molecules. Based on the comparative molecular field analysis model, new compounds were designed by LeapFrog. Seven new compounds with improved binding energy and predicted activities were finally obtained.

Key words: molecular design, molecular docking, neuraminidase inhibitors, QSAR, thiourea and thiadiazolo [2,3-a] pyrimidine derivatives

Received 4 August 2009, revised 3 April 2010 and accepted for publication 30 May 2010

Neuraminidase (NA) is one of the two glycoproteins on the surface of influenza virus, and NA is responsible for viral release from infected cells and viral transport through the mucus in the respiratory tract (1). Neuraminidase has been found to be a potential target to control influenza virus (2). Neuraminidase inhibitors (NIs) form key components of pandemic preparedness plans as treatment and prophylaxis could reduce virus transmission (3). Sialic acid analogues are NIs that reported most early. Then, different series of NIs were prepared, such as cyclohexene (4), benzoic acid (5), pyrolidine derivates (6,7), and so on. During the past decade, thiourea derivatives have been reported to be effective against HIV and to have bactericidal action (8). But few studies have been carried out concerning evaluations of substituted acyl(thio)urea and 2H-1,2,4-thiadiazolo [2,3-α] pyrimidine for their antiviral activity (8). In 2006, a new class of substituted acyl(thio)urea and 2H-1,2,4-thiadiazolo [2,3-α] pyrimidine derivatives were prepared by Sun *et al.* (8). A highly specific anti-influenza virus activity in cell culture was discovered. *In vitro* inhibitory activities of influenza neuraminidase (H1N1) were also investigated and found to correlate well with their antiviral efficacy in cell culture (8).

To develop potent antiviral agents, quantitative structure–activity relationship (QSAR) studies of NIs have been carried out by many researchers. For example, comparative molecular similarity indices analysis (CoMSIA) studies of cyclohexene, cyclopentane, pyrolidine, and benzoic acid derivatives were reported by Yi *et al.* (9). Based on docking conformations, q^2 of four optimal QSAR models were 0.701 with nine optimal principal components (steric and electrostatic), 0.562 with 11 optimal principal components (steric, electrostatic and hydrophobic), 0.704 with 14 optimal principal components (steric, electrostatic, and hydrogen bond), and 0.651 with ten optimal principal components (steric, electrostatic, hydrophobic, and hydrogen bond). In 2006, based on physicochemical and electronic

Table 1: Structures, experimental activities, predicted activities, and docking scores of 36 NIs

ID	R	X	Y	Exp. pIC_{50} (M)	Pred. pIC_{50} (M)			Total Scores	CScore	Hydrogen bond numbers
					HQSAR	CoMFA	CoMSIA			
1*	2-Cl	OEt	Me	5.78	6.03	6.45	6.14	4.11	3	6
2	2-Cl	OEt	OEt	7.10	6.80	6.85	7.03	8.33	4	9
3	2-Cl	OH	Me	6.49	6.38	6.74	6.70	4.80	3	6
4	2-Cl	OMe	OMe	5.75	5.92	5.76	5.74	4.81	3	6
5*	2-Cl	Cl	Cl	4.84	5.58	5.30	5.48	2.04	4	5
6	4-NO_2	Cl	Cl	5.78	5.90	5.95	6.02	3.22	4	3
7*	4-NO_2	OEt	Me	5.64	6.20	6.22	6.40	3.49	4	4
8	4-NO_2	OH	Me	6.44	6.35	6.26	6.21	3.82	3	6
9	5-(2-Cl-Ph)-2-furyl	–	–	5.85	6.01	5.77	5.72	5.09	5	7
10	5-(4-NO_2-Ph)-2-furyl	–	–	5.89	5.98	5.78	5.67	4.32	3	7
11*	Ph	–	–	5.75	6.28	5.48	5.71	3.92	4	5
12	OMe	–	–	5.74	5.89	5.95	5.86	4.78	3	7
13	(2,4-Cl_2-Ph)-OCH_2	–	–	5.78	5.59	5.93	5.80	3.55	3	7
14	2,6-F_2-Ph	–	–	5.84	5.59	5.75	5.85	3.89	5	7
15	S-(+)2-Me-1-(4-Cl-Ph)-Pr	–	–	5.87	5.94	5.95	5.83	4.80	3	6
16	cis-(-)CFPC	–	–	6.29	6.29	6.39	6.15	5.21	5	8
17*	trans-(-)DCPC	–	–	6.59	6.30	6.96	6.16	5.47	4	7
18	5-(4-NO_2-Ph)-2-furyl	OMe	Me	5.91	5.99	5.71	5.65	4.37	5	7
19	5-(2-Cl-Ph)-2-furyl	OMe	Cl	5.89	5.94	5.66	5.67	4.38	3	6
20	6-Cl-3-pyridyl	Me	OH	5.07	5.17	5.14	5.17	2.66	4	5
21	2-Cl-3-pyridyl	Me	Me	5.14	5.32	5.30	5.35	2.95	4	5
22	2-Cl-3-pyridyl	OMe	Cl	5.59	5.17	5.31	5.31	3.27	3	7
23	5,6-Cl_2-3-pyridyl	OMe	OMe	4.73	4.92	5.05	4.96	2.10	4	6
24*	Ph	Me	Me	5.68	5.71	5.69	5.55	3.66	3	4
25	2-Me-1-(4-Cl-Ph)-Pr	OEt	OEt	6.51	6.53	6.57	6.52	5.98	4	5
26	CFPC	OMe	OMe	6.01	5.97	5.73	5.90	4.16	4	5
27	CFPC	Me	Me	6.24	6.31	6.29	6.27	4.72	5	5
28	2-F-4-Cl-Ph	Me	Me	5.87	5.64	5.65	5.66	4.05	3	4
29	2-F-4-Cl-Ph	OMe	Cl	5.29	5.49	5.50	5.67	3.49	5	4
30*	(2,4-Cl_2-Ph)-OCH_2	OMe	OMe	5.72	5.32	6.18	6.17	4.49	3	3
31	5-(4-NO_2–Ph)–2-Furyl	Me	OH	6.17	6.26	6.33	6.36	3.83	4	9
32*	5-(4-NO_2–Ph)–2-Furyl	OEt	OEt	5.28	5.90	6.02	5.82	2.77	3	4
33	5-(2-Cl–Ph)–2-Furyl	OEt	Me	6.46	6.56	6.45	6.53	6.24	3	8
34	6-Cl-3-pyridyl	OMe	Cl	5.03	4.93	5.18	5.36	2.54	4	2
35*	6-Cl-3-pyridyl	OEt	OEt	7.04	6.83	6.82	6.73	4.92	5	6
36	2-Cl-3-pyridyl	OMe	OMe	5.62	5.54	5.41	5.40	4.03	4	3
37	zanamivir (GG167)	–	–	–	5.71	5.96	5.91	7.73	5	9

CoMFA, comparative molecular field analysis; CoMSIA, comparative molecular similarity indices analysis; HQSAR, hologram quantitative structure–activity relationship

*Samples in test set; Total Sores: Surflex–Dock scores are expressed in $-\log_{10}(K_d)$ units to represent binding affinities.

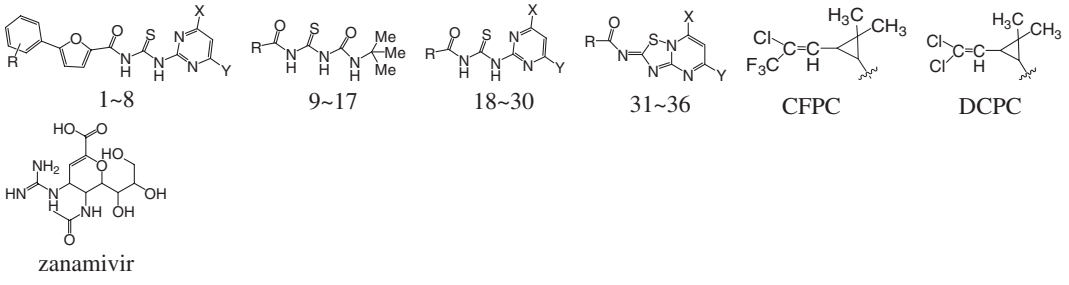

Scheme 1: Various molecular skeletons. 1∼8 (polysubstituted pyrimidinyl acyl(thio)urea analogues); 9∼17 (tert-butylaminocarbonyl acyl(thio)urea analogue); 18∼30 (aryl and chrysanthemoyl R groups); 31∼36 (2H-1,2,4-thiadiazolo [2,3-a] pyrimidine ring); CFPC (3-(2-chloro-3,3,3-trifluropropenyl)-2,2-dimethyl cyclopropyl); DCPC (3-(2,2-dichloro ethenyl)-2,2-dimethyl cyclopropyl); zanamivir (37: GG167).

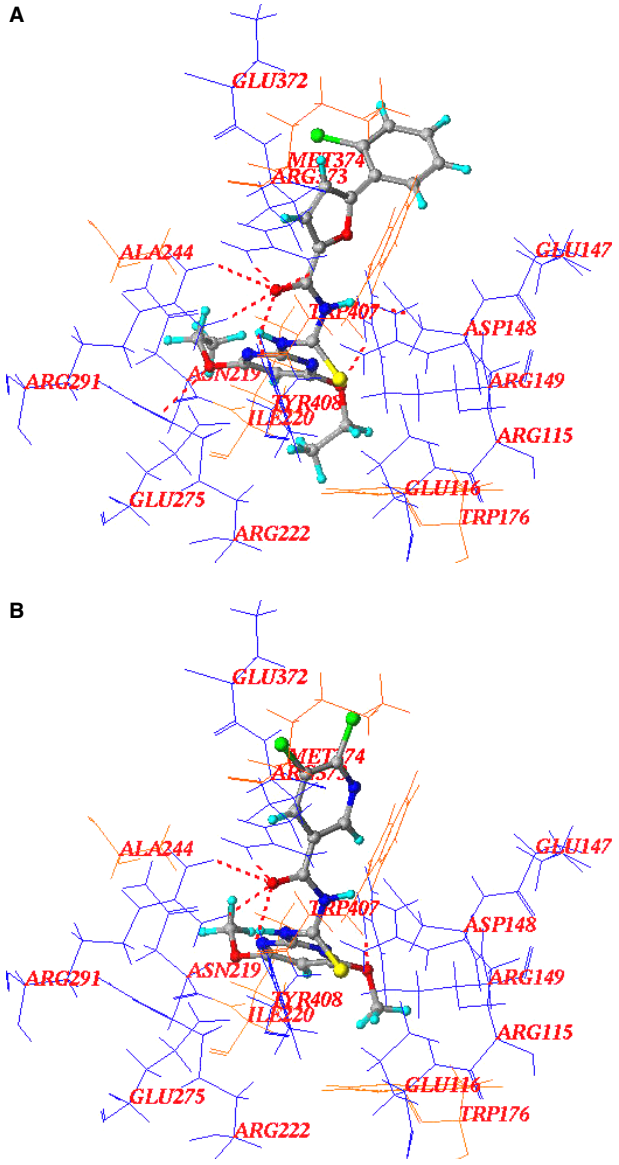

Figure 1: Hydrogen bonding interactions (dashed line) between samples ID 2 (A), ID 23 (B) and key amino acid residues in the active site.

parameters, QSAR of benzoic acid, carbocyclic ring, cyclopentane, and isoquinoline derivatives was investigated by Rajeshwar *et al.* (2), and 17 QSAR models with good statistical results were obtained. Quantitative structure–activity relationship models of 46 NIs consisting of cyclohexene, cyclopentane, pyrolidine, and benzoic acid derivatives were established by heuristic method (HM) and radial basis function network (RBFNN), reported by Lü *et al.* (10). The result of linear HM model indicated that hydrophobicity and hydrogen bond interactions played important roles in the activities of NIs. Non-linear RBFNN models produced better results with good predictive capability than the linear HM model. Based on spatial, topological, electronic, thermodynamic, and E-state indices, QSAR of 40 thiourea analogues was investigated by Nair *et al.* (11). A statistically significant model with five variables was obtained using

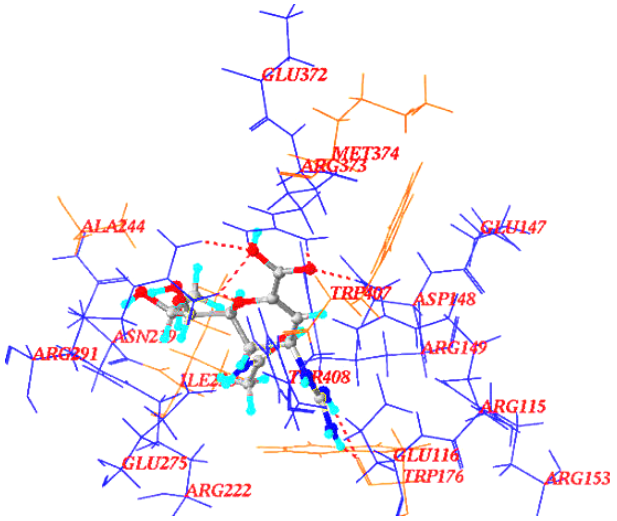

Figure 2: Hydrogen bonding interactions (dashed line) between the position calculated of zanamivir crystal structure and key amino acids in the active site.

genetic algorithms. The results revealed that the atom type logP and shadow indices (spatial indices) were the dominant features affecting NA inhibitory activities.

In this paper, molecular docking, hologram quantitative structure–activity relationship (HQSAR), comparative molecular field analysis (CoMFA), and CoMSIA were employed to investigate ligand–receptor interactions and construct QSAR models of 48 thiourea and thiadiazolo [2,3-α] pyrimidine derivatives (8). Based on the CoMFA model, new compounds with improved binding energy were designed by LeapFrog. Designed compounds were further selected by QSAR models and docking.

Methods and Materials

Surflex–Dock in SYBYL 7.3 (Tripos, Inc., St. Louis, MO, USA) that was applied to study molecular docking uses an empirical scoring function and a potent search engine to dock ligands into a protein's binding site (12). A *Protomol* (13) that is used to guide molecular docking is a computational representation of the receptor's binding cavity to which putative ligands are aligned. A *Protomol* can be generated automatically or defined based on a cognate ligand or known active site. In this paper, a *Protomol* was automatically generated. Two parameters determining the extent of a *Protomol*, threshold parameter of 0.31, and bloat parameter of 1 Å were established. The total Surflex–Dock score was expressed as $-\log_{10}(K_d)$ to represent binding affinities. The strengths of individual scoring functions combine to produce a consensus that is more robust and accurate than any single function for evaluating ligand–receptor interactions. So, CScore (Consensus Score) (14) was used for ranking the affinity of ligands bound to the active site of a receptor. CScore integrates a number of popular scoring functions and provides several functions: D_Score (15), Potential of Mean Force (PMF)_Score (16), G_Score (17), and CHEM Score (18). CScore ranges from 1 to 5, and the best is 5.

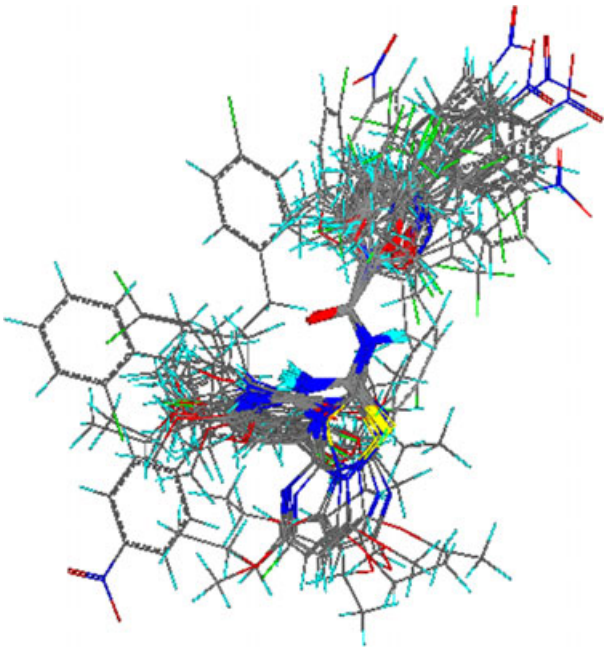

Figure 3: Receptor-based alignment plot of 36 samples in the active site of neuraminidase.

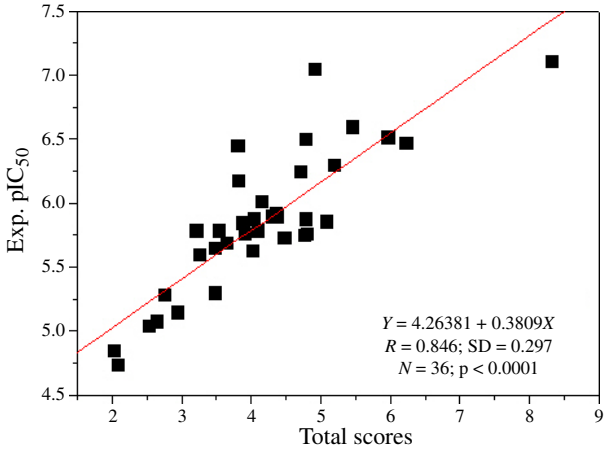

Figure 4: The correlation between the total scores and the experimental activities of neuraminidase inhibitors.

In this paper, crystal structure of NA with zanamivir (GG167) was retrieved from Protein Data Bank (entry code: 1a4g) (19). 1a4g is a dimer of two chains. Only the monomeric unit was used in docking studies. Preparation of receptor (1a4g) is as follows: all the water molecules were deleted; hydrogens (20,21) and AMBER7 FF99 charges were added. The protein structure was utilized in subsequent docking experiments without energy minimization. In addition, disposal of ligands (samples) is given later: the method of energy minimization was Powell; force field and charge were Tripos and MMFF94; max iterations, termination, and RMS displacement were 1000, 0.001 kcal/(mol*Å), and 0.001 Å, respectively; other parameters were established using default values.

Hologram quantitative structure–activity relationship ([a–c]), CoMFA (22), and CoMSIA (23,24) were applied to establish QSAR models. The premise of HQSAR is that the structure of a molecule is encoded within its 2D fingerprint and structure is the key determinant of all molecular properties. During HQSAR modeling, information of fragments including atoms, bonds, connections, hydrogen atoms, chirality, hydrogen bond donor, and acceptor was considered. Fragment size of default 4-7 and default 12 hologram lengths (53, 59, 61, 71, 83, 97, 151, 199, 257, 307, 353, and 401) was used. Based on the least standard error, the best HQSAR model was selected by PLS.

Molecular conformations with the highest total scores were used in CoMFA and CoMSIA (21) studies. Based on the receptor, all 36 samples were aligned. In addition, Clogp was used to represent hydrophobic interaction during CoMFA modeling. Comparative molecular field analysis and CoMSIA parameters were established by default. Comparative molecular field analysis and CoMSIA models were generated by Sample-distance partial least squares (SAMPLS) (25). All QSAR models were validated by leave-one-out cross-validation (LOO CV) and external prediction by test set (r^2_{test}).

As a second generation *de novo* drug discovery method, LeapFrog performs electrostatic screening, by repeatedly making some structural change and then either keeping or discarding the results, depending on the evolution (26,27). LeapFrog can run in three alternative modes: (i) OPTIMIZE suggests improvements to existing leads; (ii) DREAM proposes new molecules expected to have good binding; and (iii) GUIDE supports interactive design by performing and evaluating user modifications. In this paper, the most active sample ID 2 was taken as a template to design new molecules (28,29). Based on the optimal CoMFA model, new compounds with high predicted inhibitory activities had been designed using OPTIMIZE mode. WEED and CROSSOVER modules were performed after the initial run of 1000 moves, and the derived ligands with the best binding energy were used for the repeating cycle of 1000 moves. When a WEED occurs, if the number of ligands is greater than 10, the ligands present are sorted by binding energy or score, and all except the top 10 are deleted. CROSSOVER is a genetic move for generating the best hybridizations among these diverse structural changes. New compounds with the constraint of synthetic difficulties were evaluated by the binding affinities during the seeking procedure. Calculation of binding energy in LeapFrog has three major components: (i) steric and electrostatic enthalpies of binding process calculated using the Tripos force field; (ii) cavity desolvation energy; and (iii) ligand desolvation energy.

Dataset

pIC_{50} (−log IC_{50}) values of 48 thiourea and thiadiazolo [2,3-α] pyrimidine derivatives were taken from reference (8). IC_{50} values were measured spectrofluorometrically using 20-(4-methylumbelliferyl)-α-D-acetylneuraminic acid as substrate for NA to yield a fluorescent product which was quantified (8). Twelve samples (IC_{50} > 20 μM) whose IC_{50} values were not quantitatively reported were deleted during modeling procedure. The remaining 36 samples were randomly divided into training set with 27 samples and test set with nine samples (Table 1 and Scheme 1).

Table 2: Statistical results and contributions of the optimal HQSAR, CoMFA, and CoMSIA models

									Contributions			
Methods	r^2	SE	q^2	SE_{CV}	F	A	r^2_{test}	Clogp	Steric	Electrostatic	Hydrophobic	Donor	Acceptor
HQSAR	0.899	0.185	0.628	0.355	–	5	0.558	–	–	–	–	–	–
CoMFA	0.878	0.194	0.656	0.333	55.139	3	0.667	0.085	0.437	0.478	–	–	–
CoMSIA	0.865	0.205	0.509	0.419	48.948	3	0.566	–	0.137	0.209	0.338	0.207	0.109

CoMFA, comparative molecular field analysis; CoMSIA, comparative molecular similarity indices analysis; HQSAR, hologram quantitative structure–activity relationship; r^2, squared multiple correlation coefficient; q^2, squared cross-validated correlation coefficient; r^2_{test}, r^2 of test set; SE, standard error; SE_{CV}, cross-validated standard error; A, the number of principal components.

Results and discussions

Molecular docking

According to Figures 1 and 2, it can be seen that the interaction residues between samples and active pocket are consistent with that between zanamivir crystal structure and active pocket.

Figure 1A illustrates hydrogen bonding (dashed line) interactions between the most active sample ID 2 and residues ASP148, TYR408, ARG149, ARG222, ARG291, and ARG373 in the active pocket. Total nine hydrogen bonds of four types (including *-N···H-O-*, *-O···H-N, =O···H-N and =O···O-H*) were formed. Figure 1B shows hydrogen bonding (dashed line) interactions between the least active sample ID 23 and residues ASP148, GLU116, ARG149, ARG291, and ARG373 in the active pocket. Total six hydrogen bonds of three types (*-O···H-N, =O···H-N, and =O···O-H*) were observed. Hydrogen bond numbers of other samples are given in Table 1. From Table 1, it can be seen that hydrogen bond numbers of samples are correlated with their pIC_{50} values, with correlation coefficient $r = 0.498$ and $p = 0.00199$.

In Figure 2, total nine hydrogen bonds of two types (including *-O···H-N- and =O···H-N-*) can be seen between the position calculated of zanamivir (GG167) crystal structure and residues ARG115, ARG149, TRP176, ARG291, and ARG373 in the active pocket. Hydrogen bonds are mainly formed between carboxy group, acyl group and guanidyl in zanamivir and residues in the active pocket.

From Figures 1 and 2, it can be seen that there are hydrophobic interactions, because there are hydrophobic residues in the active pocket. In Figures 1 and 2, it can be observed that the residues in the active pocket are main hydrophilic and polar residues. Therefore, electrostatic interactions can be observed between NIs, zanamivir, and residues in the active pocket.

Figure 3 depicts receptor-based alignment plot of all 36 samples. It is evident that the docked samples align well, especially in the region of the amide bond. It suggests that docking model of samples may have some similarity. Moreover, there is a strong correlation between binding affinity (total scores) and experimental pIC_{50} values with correlation coefficient $r = 0.846$, SD = 0.297, and $p < 0.0001$ (Figure 4). This suggests that docking results can characterize the mode of ligand–receptor interactions to some extent.

HQSAR, CoMFA and CoMSIA

Statistical results of HQSAR, CoMFA, and CoMSIA models are given in Table 2, and the predicted pIC_{50} values are shown in Table 1. From Table 2, it can be seen that q^2 and r^2_{test} of three QSAR models are 0.628, 0.558, and 0.656 and 0.667, 0.509, and 0.566, respectively (Figures 5 and 6). The results show that the QSAR models are robust and have predictive capabilities.

From Figures 5 and 6, it can be seen that models have low predictive ability, which predicted samples with low activities. In Figure 5, all samples were uniformly distributed around diagonal except ID 5. The reason might be lower activity of ID 5 in comparison with that of other samples. But all samples were nearly uniformly distributed around diagonal in Figure 6.

In the HQSAR model, the molecule is color coded to reflect the individual atomic contributions to the activities. The colors at the red end of the spectrum (red, red orange, and orange) reflect poor (or negative) contributions, while colors at the green end (yellow, green blue, and green) reflect favorable (positive) contributions. Atoms with intermediate contributions are colored white. Figure 7 shows the individual atomic contributions of samples ID 1∼5. The numbers of green atoms in these five samples are 3, 4, 3, 0, and 0, respectively. From the results, it can be seen that the numbers

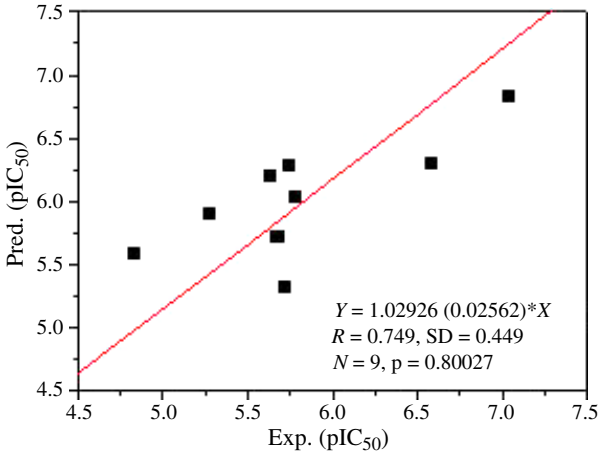

Figure 5: The linear regression plots of experimental versus predicted pIC_{50} values of samples in test set through origin (Hologram quantitative structure–activity relationship).

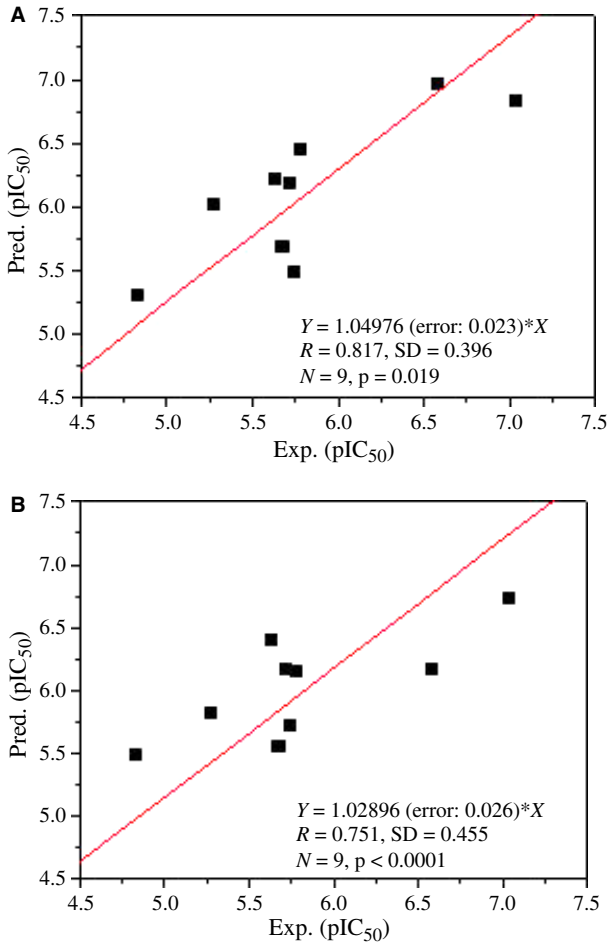

Figure 6: The linear regression plots of experimental versus predicted pIC_{50} values of samples in test set through origin (A, comparative molecular field analysis; B, comparative molecular similarity indices analysis).

of green atoms in samples are correlated with their activities in some degree. The green atoms of these five samples are mainly distributed in X and Y substituent groups. So, the modification of X and Y substituent groups should be especially focused on to improve the inhibitory activities of NIs.

Comparative molecular field analysis steric and electrostatic contour maps are given in Figure 8 (reference molecule: ID 2). Favored and disfavored levels fixed at 80% and 20%, respectively. In CoMFA steric contour map (Figure 8A), the favorable large bulk regions are green, whereas the unfavorable large bulk regions are yellow. From contour maps, there are large green regions around R and Y substituent groups. For example, activity of sample ID 2 is higher than that of sample ID 1, because bulk of Y substituent group of sample ID 2 is larger than that of sample ID 1. Similar conclusions can be drawn from ID 5 to 6, ID 9–10, ID 34–36, and so on. There are yellow regions around X substituent groups, which suggest that X substituent group with a small bulk can enhance activity; for example, activity of sample ID 3 is higher than that of sample ID 1. Similar conclusions can be drawn from ID 3 to 4, ID 7–8, and so forth.

In CoMFA electrostatic contour map Figure 8B, red and blue regions are favorable to improve activity when substituent groups are more electropositive and more electronegative, respectively. For example, there is a large of blue regions around R and Y substituent groups, which indicate that electronegativity can increase activity. It is consistent with electrostatic interactions that are formed between electronegative atom (chlorine atom) in R and amide nitrogen in ARG 373 and MET374, between oxygen atom of furan in sample and nitrogen of indolyl in TRP 407, between electronegative atom (oxygen atom) in Y substituent group and guanidyl of residues (ARG149, ARG115). There are two red regions around acyl group and oxygen of X substituent group, which are consistent with the docking results. It can be observed that carboxy of ASP148 around amide nitrogen in sample is electronegative, carbonyl in TRP407 round amide oxygen in samples and carboxy of GLU275 around oxygen in X substituent are electronegative. It is obvious that electrostatic interactions involve in high polar/charged regions.

Comparative molecular similarity indices analysis contour maps of hydrogen bond donors and acceptors, and hydrophobicity are given in Figure 9 (reference molecule: ID 2). In Figure 9A, red regions indicate that hydrogen bond donor is of advantage to improve activity, whereas green regions are disadvantageous. The favorable hydrogen bond receptors regions are cyan; however, the unfavorable hydrogen bond receptors regions are yellow. For example, in cyan regions, Y substituent group of sample ID 2 is ethoxy, but Y substituent group of sample ID 1 is methyl. However, ethoxy oxygen is helpful to form hydrogen bond acceptor. Consequently, activity of sample ID 2 is higher than that of sample ID 1. Similar conclusions can be drawn from ID 4 to 5, ID 9–10, ID 34–36, and so on.

In Figure 9B, the favorable hydrophobic regions are red, for instance, activity increases were seen from ID 1 to 2, ID 11–12, ID

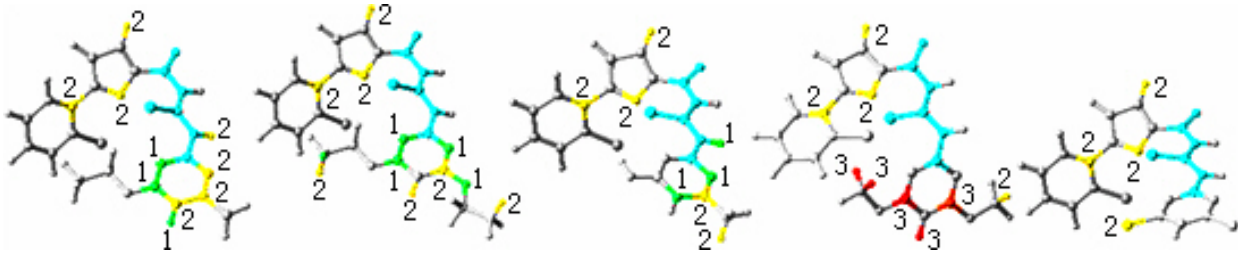

Figure 7: The individual atomic contributions to the bioactivity of 5 samples (ID: 1~5; 1, 2 and 3 represent green, yellow and red atoms, respectively).

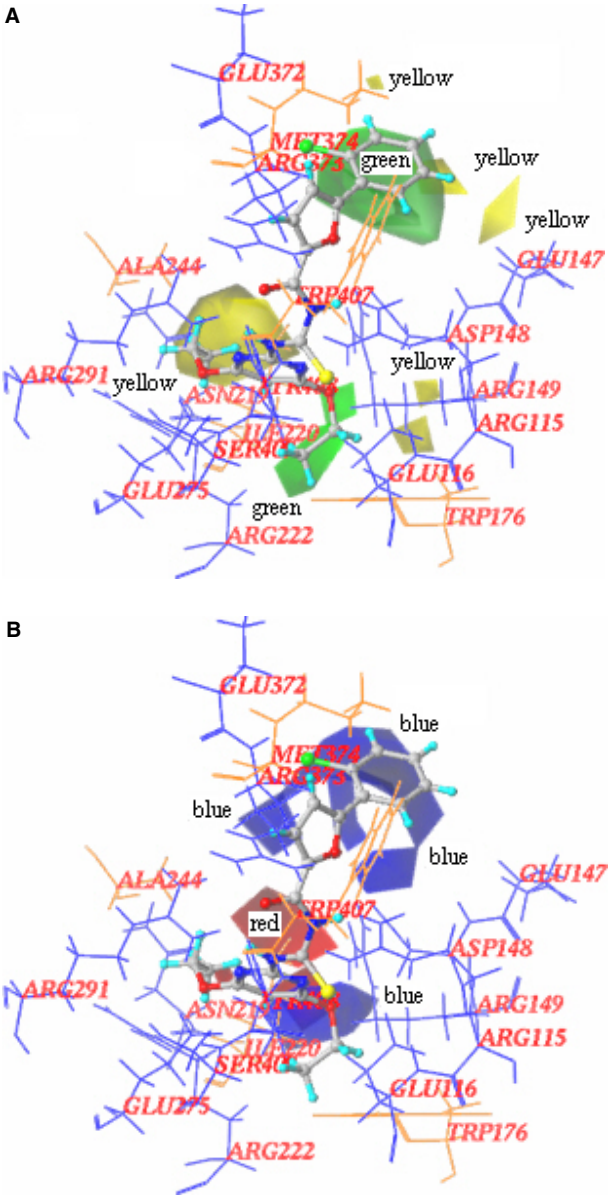

Figure 8: Comparative molecular field analysis steric (A) and electrostatic (B) contour maps (The contours of the steric map are shown in yellow and green, and those of the electrostatic map are shown in red and blue. Greater activity values are correlated with: more bulk near green, less bulk near yellow, more positive charge near blue, and more negative charge near red. Reference molecule: ID 2).

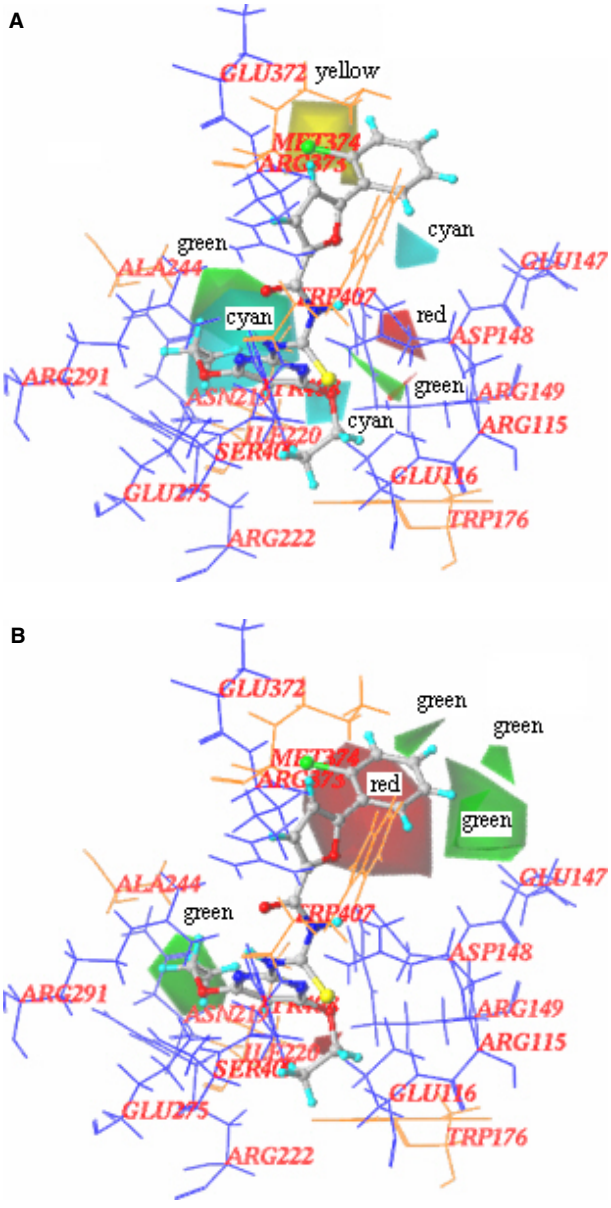

Figure 9: Comparative molecular similarity indices analysis contour maps for hydrogen bond donor and acceptor (A), hydrophobicity (B). (A: the favorable hydrogen bond donor areas are red, and the unfavorable hydrogen bond donor areas are green; the favorable hydrogen bond receptors regions are cyan, the unfavorable hydrogen bond receptors regions are yellow. B: the favorable hydrophobic areas are red, and the unfavorable hydrophobic areas are green. Reference molecule: ID 2).

20–21, and so on, whereas the unfavorable hydrophobic regions are green, for example, activity decreases were observed from ID 4 to 5, ID 6–5, and so forth. Red regions are mainly distributed around R substituent group, and a small of red region is distributed around Y substituent group. It is obvious that results of CoMSIA hydrophobic contour maps are consistent with hydrophobic interactions that are formed between residues (TRP176 and ILE220) and Y substituent group, between residues (MET374 and TRP407) and R substituent group. However, there are two green regions around residues ARG291, ASN219, TYR408, GLU275, ARG222, and GLU147, which are mainly distributed around X substituent group and partially R substituent group. Comparative molecular similarity indices analysis steric and electrostatic contour maps are similar to that of CoMFA.

In conclusion, R and Y substituent groups with large bulk, hydrophobicity and electronegativity increase inhibition NA. X substituent

groups with small bulk and hydrophilicity also favor strong inhibition NA. Comparative molecular field analysis and CoMSIA results are internally consistent, showing usefulness of the docking. So, these groups and atoms can be modified to obtain new compounds.

Molecular design

Based on the CoMFA model, the most active sample ID 2 was taken as a template to design new compounds. New compounds with improved binding energy were obtained. The designed com-

Table 3: Structures, predicted activities, and docking scores of designed compounds

ID	Structures	Experimental pIC_{50}	Predicted pIC_{50}			LeapFrog binding energy (kcal/mol)	Total Scores	CScore
			HQSAR	CoMFA	CoMSIA			
2	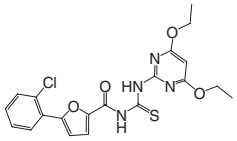	7.10	6.80	6.85	7.03	−1010.06	8.33	4
2a	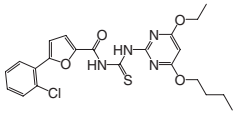	–	6.93	7.22	7.19	−1242.22	8.15	3
2b	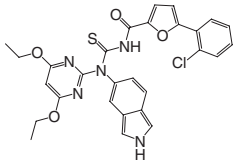	–	7.13	7.05	7.00	−1008.05	8.80	4
2c	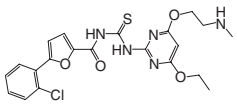	–	6.79	6.95	7.18	−1102.31	8.56	5
2d	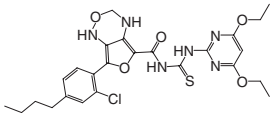	–	7.08	6.95	7.02	−1014.57	4.66	5
2e	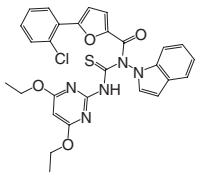	–	6.83	6.92	7.09	−1024.91	8.91	3
2f	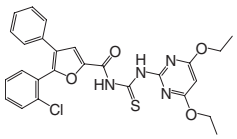	–	7.38	6.88	7.54	−1016.48	9.10	4
2g	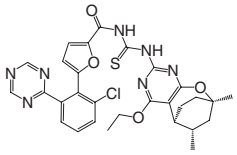	–	7.26	6.88	7.21	−1018.02	7.95	3

CoMFA, comparative molecular field analysis; CoMSIA, comparative molecular similarity indices analysis; HQSAR, hologram quantitative structure–activity relationship

pounds were further selected by QSAR models and docking. So, total seven new compounds had been finally chosen (Table 3). From Table 3, it could be observed that increase in hydrophobic, hydrogen bonding, electrostatic, and steric interactions results in enhancement of predicted inhibitory activities of designed compounds. For example, Y substituent group of the compound 2a was $-O(CH_2)_3CH_3$, but the template molecule ID 2 was $-OCH_2CH_3$. Activity of the compound 2a was enhanced along with increase in hydrophobic and steric interactions. Except the compound 2d, total scores of 4 new designed compounds (namely 2b, 2c, 2e, and 2f) were higher than that of the template molecule, and total scores of the compounds 2a and 2g were close to that of the template molecule. The structures of these seven compounds along with their binding energies, docking scores and predicted activities are given in Table 3.

Conclusions

Docking results of 36 polysubstitution thiourea and thiadiazolo [2,3-α] pyrimidine derivatives show that hydrogen bonding, electrostatic, and hydrophobic interactions are important features affecting activities of these inhibitors. Moreover, there is a significant correlation between docking total scores and experimental pIC_{50} values, with coefficient correlation $r = 0.846$ and $p < 0.0001$. Hologram quantitative structure–activity relationship is applied to develop QSAR model. r^2 and q^2 of the HQSAR model are 0.899 and 0.628, respectively. Based on receptor alignment, CoMFA and CoMSIA models were obtained. r^2 and q^2 of two models are in turn 0.878 and 0.656, 0.865 and 0.509. In addition, r^2_{test} of the HQSAR, CoMFA, and CoMSIA models are 0.558, 0.667, and 0.566, respectively. Comparative molecular field analysis and CoMSIA results show R and Y substituent groups with large bulk, electronegativity and hydrophobicity increase NA inhibition. X substituent groups with small bulk and hydrophilicity can enhance inhibitory activity. Furthermore, QSAR results were consistent with the docking results. Based on the CoMFA model, seven new compounds with improved binding energy and predicted inhibitory activity were finally obtained. Except one new compound, total scores of four new compounds are higher than that of the template molecules, and total scores of two new compounds are close to that of the template molecules.

Acknowledgments

The authors thank professor Gang Chen in National Technology College of Singapore for offering us docking results of the sybyl program and help. This work was supported by the national high technology research and development program of China (Grant No. 2006AA02Z312) and Chongqing University postgraduates' innovative team building project (Grant No. 200909b1008).

References

1. McKimm-Breschkin J.L. (2000) Resistance of influenza viruses to neuraminidase inhibitors – a review. Antiviral Res;47:1–17.
2. Verma R.P., Hansch C. (2006) A QSAR study on influenza neuraminidase inhibitors. Bioorg Med Chem;14:982–996.
3. Stephenson I., Clark T.W., Pareek M. (2008) Antiviral treatment and prevention of seasonal influenza: A comparative review of recommendations in the European Union. J Clin Virol;42:244–248.
4. Kim C.U., Lew W., Williams M.A., Wu H., Zhang L.J., Chen X.W., Escarpe P.A., Mendel D.B., Graeme Laver W., Stevens R.C. (1998) Structure-activity relationship studies of novel carbocyclic influenza neuraminidase inhibitors. J Med Chem;41:2451–2460.
5. Brouillette W.J., Atigadda V.R., Luo M., Air G.M., Babu Y.S., Bantia S. (1999) Design of benzoic acid inhibitors of influenza neuraminidase containing a cyclic substitution for the N-acetyl grouping. Bioorg Med Chem Lett;9:1901–1906.
6. Wang G.T., Chen Y.W., Wang S., Gentles R., Sowin T., Kati W., Muchmore S., Giranda V., Stewart K., Sham H., Kempf D., Laver W.G. (2001) Design, synthesis, and structural analysis of influenza neuraminidase inhibitors containing pyrrolidine cores. J Med Chem;44:1192–1201.
7. Krueger A.C., Xu Y.B., Kati W.M., Kempf D.J., Maring C.J., McDaniel K.F., Molla A., Montgomery D., Kohlbrenner W.E. (2008) Synthesis of potent pyrrolidine influenza neuraminidase inhibitors. Bioorg Med Chem Lett;18:1692–1695.
8. Sun C.W., Zhang X.D., Huang H., Zhou P. (2006) Synthesis and evaluation of a new series of substituted acyl(thio)urea and thiadiazolo [2,3-a] pyrimidine derivatives as potent inhibitors of influenza virus neuraminidase. Bioorg Med Chem;14:8574–8581.
9. Yi X., Guo Z., Chu F.M. (2003) Study on molecular mechanism and 3D-QSAR of influenza neuraminidase inhibitors. Bioorg Med Chem;11:1465–1474.
10. Lü W.J., Chen Y.L., Ma W.P., Zhang X.Y., Luan F., Liu M.C., Chen X.G., Hu Z.D. (2008) QSAR study of neuraminidase inhibitors based on heuristic method and radial basis function network. Eur J Med Chem;43:569–576.
11. Nair P.C., Sobhia M.E. (2008) Quantitative structure activity relationship studies on thiourea analogues as influenza virus neuraminidase inhibitors. Eur J Med Chem;43:293–299.
12. Jain A.N. (2003) Surflex: fully automatic flexible molecular docking using a molecular similarity-based search engine. J Med Chem;46:499–511.
13. Ruppert J., Welch W., Jain A.N. (1997) Automatic identification and representation of protein binding sites for molecular docking. Protein Sci;6:524–533.
14. Clark R.D., Strizhev A., Leonard J.M., Blake J.F., Matthew J.B. (2002) Consensus scoring for ligand/protein interactions. J Mol Graph Model;20:281.
15. Jones G., Willet P., Glen R.C., Leach A.R., Taylor R. (1997) Development and validation of a genetic algorithm for flexible docking; J. Mol Biol;267:727.
16. Muegge I., Martin Y.C. (1999) a general and fast scoring function for protein-ligand interactions: a simplified potential approach. J Med Chem;42:791–804.
17. Kuntz I.D., Blaney J.M., Oatley S.J., Langridge R., Ferrin T.E. (1982) A geometric approach to macromolecule-ligand interactions. J Mol Biol;161:269–288.
18. Eldridge M.D., Murray C.W., Auton T.R., Paolini G.V., Mee R.P. (1997) Empirical scoring functions: I. The development of a fast empirical scoring function to estimate the binding affinity of

ligands in receptor complexes. J Comput Aided Mol Des;11:425–445.
19. Taylor N.R., Cleasby A., Singh O., Skarzynski T., Wonacott A.J., Smith P.W., Sollis S.L., Howes P.D., Cherry P.C., Bethell R., Colman P., Varghese J. (1998) Dihydropyrancarboxamides related to zanamivir: a new series of inhibitors of influenza virus sialidases. 2. Crystallographic and molecular modeling study of complexes of 4-amino-4H-pyran-6-carboxamides and sialidase from influenza virus types A and B. J Med Chem;41:798–807.
20. Muthas D., Sabnis Y.A., Lundborg M., Karlén A. (2008) Is it possible to increase hit rates in structure-based virtual screening by pharmacophore filtering? An investigation of the advantages and pitfalls of post-filtering J Mol Graph Model;26:1237–1251.
21. Clark R.D. (2008) A Ligand's-eye view of protein binding. J Comput Aided Mol Des;22:507–521.
22. Cramer R.D. III, Patterson D.E., Bunce J.D. (1988) Comparative molecular field analysis (CoMFA). 1. Effect of shape on binding of steroids to carrier proteins. J Am Chem Soc;110: 5959–5967.
23. Klebe G., Abraham U. (1999) Comparative Molecular Similarity Index Analysis (CoMSIA) to Study Hydrogen Bonding Properties and to Score Combinatorial Libraries. J Comput Aided Mol Des;13:1–10.
24. Böhm M., Stürzebecher J., Klebe G. (1999) 3D QSAR Analyses using CoMFA and CoMSIA to Elucidate Selectivity Differences of Inhibitors Binding to Trypsin, Thrombin and Factor Xa. J Med Chem;42:458–477.
25. Bush B.L., Nachbar R.B. (1993) Sample-Distance Partial Least-Squares-PLS Optimized for Many Variables, with Application to CoMFA. J Comput Aided Mol Des;7:587–619.
26. Payne A.W.R., Glen R.C. (1993) Molecular Recognition Using a Binary Genetic Search Algorithm. J Mol Graph;11:74.
27. Dixon S., Blaney J., Weininger D. (1993) Presented at the Third York Meeting - Characterizing and Satisfying the Steric and Chemical Restraints of Binding Sites; March: 29–30.
28. Nair P.C., Sobhia M.E. (2007) CoMFA based de novo design of pyridazine analogs as PTP1B inhibitors. J Mol Graph Model;26:117–123.
29. Kumar A., Siddiqi M.I. (2008) CoMFA based de novo design of Pyrrolidine Carboxamides as Inhibitors of Enoyl Acyl Carrier Protein Reductase from Mycobacterium tuberculosis. J Mol Model;14:923–935.

Notes

[a]Barnard J.M., Downs G.M. (1995) Fingerprint Descriptor Package, 3.1; Barnard Chemical Information Ltd.: Sheffield.
[b]James C.A., Weininger D. (1995) Daylight Theory Manual; Daylight Chemical Information Systems, Inc.
[c]UNITY Reference Manual; Tripos Inc.: St.Louis, MO (1995).